The Journal of Supercritical Fluids xxx (xxxx) 107065

Contents lists available at ScienceDirect

The Journal of Supercritical Fluids

journal homepage: www.elsevier.com

Application of supercritical carbon dioxide to the synthesis of diverse surface-modified metal oxide nanoparticles

Wenjing Hu [a, b], Aoi Muronosono [a], Yuki Yamaguch [a], Yi Liu [b], Yusuke Shimoyama [a], Yasuhiko Orita [a, *]

[a] Department of Chemical Science and Engineering, Institute of Science Tokyo, 2-12-1 S1-33, Ookayama, Meguro-ku, Tokyo 152-8550, Japan
[b] State Key Laboratory of Fine Chemicals, School of Chemical Engineering, Dalian University of Technology, Dalian, China

ARTICLE INFO

Keywords:
Supercritical carbon dioxide
Green synthesis
Metal oxide nanoparticles
Surface modification
Phase analysis

ABSTRACT

Supercritical CO_2 ($scCO_2$) is an appealing medium for the green synthesis of surface-modified metal oxide nanoparticles (MONPs) owing to its nontoxicity, low cost, and recyclability. However, the synthesis of MONPs using $scCO_2$ is currently limited to iron oxide systems, and their application to other metal oxide systems has not been sufficiently explored. In this study, we aim to demonstrate the universality of $scCO_2$ synthesis method for various surface-modified MONPs. The synthesis and phase analysis were performed at 30.0 ± 0.5 MPa of CO_2 and 100 °C for 18 h, utilizing metal acetylacetonate, water, oleic acid, and ethanol as reactants. As a result, α-Fe_2O_3, TiO_2, and CeO_2 nanocrystals were successfully synthesized from $Fe(acac)_3$, $TiO(acac)_2$, and $Ce(acac)_3$, respectively. Notably, incorporating oleic acid into $scCO_2$ effectively inhibited the aggregation of α-Fe_2O_3, TiO_2, and CeO_2 nanocrystals through chemical modification of their surfaces. Additionally, phase and metal oleate analyses suggested that the successful formation of metal oleate intermediates and their subsequent hydrolysis in the homogeneous $scCO_2$ phase are key to the synthesis of densely modified MONPs. These results demonstrate that $scCO_2$ is a promising medium for the efficient synthesis of diverse surface-modified MONPs with minimal solvent usage and zero pollution.

1. Introduction

Metal oxide nanoparticles (MONPs) have garnered significant research interest across diverse scientific disciplines and industrial applications owing to their unique physicochemical properties [1]. However, the inherently high surface energy of MONPs causes them to aggregate spontaneously, limiting their practicality in advanced applications [2–4]. Surface-modified MONPs, in which organic surfactants chemically attach to the surface via covalent bonding, are attractive alternatives because surface modification significantly decreases their inherent surface energy, suppressing interparticle aggregation and enhancing solvent compatibility via tailored surface hydrophilicity and hydrophobicity [5,6]. These optimized physicochemical properties enable the application of MONPs in diverse fields, including biomedicine [7], engineering [8], catalysis [9,10], optoelectronics [11,12], and food technology [13,14].

In recent years, considerable attention has been paid to the solution-based synthesis of surface-modified MONPs using various strategies, including sol–gel [15], hot injection [16], template-assisted [17], heat-up [18], and hydrothermal methods [19]. Although recent research has focused on the design and fabrication of nanoparticle-containing composites and hybrid materials, the development of uniform surface-modified MONPs as fundamental building blocks remains crucial [20,21]. Uniform NPs with controlled surfaces offer excellent dispersibility and functionality and serve as fundamental building blocks for constructing advanced nanocomposites with practical applicability [22,23]. Despite the superior morphological and surface functional control achieved via liquid-phase routes, their sustainability remains a challenge, mainly owing to the use of large amounts of toxic solvents for production and cleaning and the treatment and recycling of subsequent waste liquids [24–27]. Owing to the avoidance of liquid waste and post-treatment, gas-phase synthesis techniques, including chemical vapor deposition [28], pulsed laser ablation [29], and thermal evaporation [30,31], have attracted significant attention for the preparation of MONPs. Nevertheless, high-temperature conditions are required for the evaporation of the precursors and pyrolytic/oxidative reactions during gas-phase synthesis, causing difficulties in surface modification and resulting in NP aggregation and low production efficiency [32,33].

* Corresponding author.
E-mail addresses: diligenliu@dlut.edu.cn (Y. Liu), yshimo@chemeng.titech.ac.jp (Y. Shimoyama), orita.y.aa@m.titech.ac.jp (Y. Orita).

https://doi.org/10.1016/j.supflu.2026.107065
Received 9 December 2025; Received in revised form 10 June 2026; Accepted 11 June 2026
0896-8446/

Owing to its nontoxicity, low cost, and recyclability, supercritical carbon dioxide ($scCO_2$) is an environmentally friendly medium that has been applied in various synthesis and extraction systems [34–37]. In addition, $scCO_2$ possesses both liquid-like solubility and gas-like diffusion characteristics, exhibiting particularly high solubility in metal precursors, which facilitates the formation of a uniform field [34,38]. These properties make $scCO_2$ an appealing medium for synthesizing surface-modified MONPs of controlled sizes [39,40]. Furthermore, $scCO_2$ enables pressure-driven separation from MONPs, eliminating additional purification/drying steps and reducing toxic solvent usage [41]. Taking these advantages into consideration, our group has developed a method to synthesize surface-modified NPs using $scCO_2$ as a reaction field [40,42]. Additionally, our group clarified the formation mechanisms of surface-modified Fe_2O_3 NPs based on the hydrolysis of metal modifier complexes and demonstrated highly concentrated synthesis by enhancing the solubility of the starting materials using an ethanol entrainer [43,44]. These findings not only pioneer the application of $scCO_2$ technology in the preparation of surface-modified MONPs but also lay a foundation for the preparation of other diverse MONPs. However, $scCO_2$ synthesis of surface-modified MONPs has been limited to iron oxide, and their applicability to other metal oxide systems (e.g., transition metal oxides and rare earth compounds) remains underexplored. Therefore, the universality of the $scCO_2$ synthesis method must be investigated to realize diverse applications of MONPs.

In this study, we aimed to demonstrate the universality of the $scCO_2$ synthesis for various surface-modified MONPs. Transition metal (Fe_2O_3, TiO_2, Co_3O_4, Cr_2O_3, NiO) and rare earth (CeO_2) oxides were selected as target metal oxide systems owing to their importance in applications such as drug delivery [7], catalysis [9,10], and electronics [11]. Metal acetylacetonate (precursor), oleic acid (surface modifier), water (oxygen donor), and ethanol (entrainer) were selected as starting materials. Metal acetylacetonates are highly stable and commercially available reagents, making them suitable metal precursors. The carboxyl group of oleic acid is suitable for the surface modification of MONPs owing to the strong covalent bonds between the carboxylate anion and metal cation [45,46]. The hydrolysis or thermolysis of metal precursors is a common reaction to synthesize MONPs using conventional hydrothermal [27] and solvothermal methods [47]. The hydrolysis of metal precursors typically proceeds at lower temperatures than thermolysis and yields metal oxide crystals relatively easily. Therefore, in this study, a small amount of water was used as the starting material to utilize the hydrolysis reaction for the synthesis of MONPs. Additionally, an ethanol entrainer was used because the addition of medium-polar solvents to $scCO_2$ can drastically enhance the solubility of medium-polar metal acetyl acetonate, polar water, and amphiphilic oleic acid with a polar carboxyl group [48], improving the uniformity of the reaction field.

2. Experimental

2.1. Materials

$Fe(acac)_3$ (>99.0%) and ethanol (>99.5%) were purchased from Wako Pure Chemicals in Japan. $TiO(acac)_2$ (>92.0%), $Co(acac)_3$ (>98.0%), $Cr(acac)_3$ (>98.0%) and oleic acid (>99.0%) were purchased from Tokyo Chemical Industry in Japan. $Ni(acac)_2$ (>95.0%) and $Ce(acac)_3$ were purchased from Sigma-Aldrich (MO in USA). CO_2 (>99.9%) and nitrogen (N_2, >99.95%) were supplied by Fujii Bussan in Japan. Ultrapure water was prepared using a Direct-Q UV3 Water Purification System supplied by EMD Millipore, and its resistivity was confirmed to be 18.2 MΩ cm.

2.2. Synthesis and phase observation

A high-pressure system was used to synthesize surface-modified MONPs in $scCO_2$ as previously described [43]. Initially, 1.5 mmol of metal acetylacetonate, 25 mmol of water, 7.5 mmol of oleic acid, and 54.3 mmol of ethanol were transferred to a 76 mL reaction vessel (TSC-CO_2–008; Taiatsu Glass). The molality of metal acetylacetonate, water, oleic acid, and ethanol corresponded to 0.03 mol kg^{-1}, 0.50 mol kg^{-1}, 0.15 mol kg^{-1}, and 1.09 mol kg^{-1}, respectively, where the molality was calculated using the volume of the vessel and CO_2 density at the reaction condition. The reaction vessel was then sealed and stirred at 500 rpm for 30 s. In the next step, the reactor was purged with CO_2 at 0.1 MPa for 1 min to remove residual gases. Liquid CO_2 was introduced using a high-performance liquid chromatography pump (PU–4386; JASCO). After pressurization to 6.0–7.0 MPa, the reactor was immersed in an oil bath and maintained under stirring at 100 °C and 30.0 ± 0.5 MPa for 18 h.

The system was depressurized at ~0.5 MPa min^{-1} through a metering valve (1315G2Y; HOKE) while cooling the vessel to ambient temperature. The products obtained from each experiment were mixed with a hexane/acetone (1:4, v/v), sonicated, centrifuged (3000 rpm for 10 min), and decanted. After repeating these washing procedure four times, the solid products obtained were dispersed in 10 mL of cyclohexane by sonication and freeze-dried to obtain the final dried powder.

To understand the reaction environment, the phase state of the reaction field was observed using a high-pressure system with a visible vessel (2.36 mL, Taiatsu Techno). Although this system, as previously described [43], differs from the synthesis equipment, the reaction conditions (100 °C, 30 MPa), concentration, and procedures were the same as those used for MONP synthesis.

2.3. Characterization

The products were observed using a transmission electron microscope (TEM) (H–7650; Hitachi) operated at 100 kV. The mean sizes and standard deviations of the particles were determined by visually estimating the boundaries of ~200 primary particles in the TEM images. High-resolution transmission electron microscopy (HR-TEM) images and TEM electron diffraction (TEM-ED) patterns of the particle colonies were obtained using a JEOL JEM–2010 F electron microscope operating at 200 kV. The solid products for TEM, HR-TEM, and TEM-ED analyses were dispersed in cyclohexane and transferred onto a copper grid with an organic membrane. Thermogravimetric analysis (TGA) was performed under an N_2 atmosphere using a thermogravimetric analyzer (DTG–60; Shimadzu); the temperature was maintained at 100 °C for 20 min and increased to 600 °C at a ramp rate of 10 °C min^{-1}. A Fourier-transform infrared (FT-IR) spectrometer (FT/IR–4X; JASCO) was used to characterize the state of the surfactant attached to the particle surface.

3. Results and discussion

3.1. Supercritical CO_2 treatment for $Fe(acac)_3$, $TiO(acac)_2$, and $Ce(acac)_3$

Surface-modified NPs of Fe_2O_3, TiO_2, and CeO_2 were synthesized from the precursors $Fe(acac)_3$, $TiO(acac)_2$, and $Ce(acac)_3$, respectively. Fig. 1 shows typical TEM images of the products synthesized with and without a surface modifier. The products synthesized without the modifier showed severe aggregation (Fig. 1**a**), whereas those synthesized with the modifier showed less aggregation (Fig. 1**b**). The Fe case gave spherical or irregularly shaped NPs, with a mean size of 5.3 ± 0.8 nm. The Ti case gave rod or ellipse-shaped NPs, with a long axis of 10.8 ± 1.8 nm and short axis of 1.6 ± 0.6 nm, where the morphology was also confirmed from the enlarged TEM images in Fig. S1. Ce case gave spherical nanoclusters with sizes of less than 5 nm and vague boundaries,

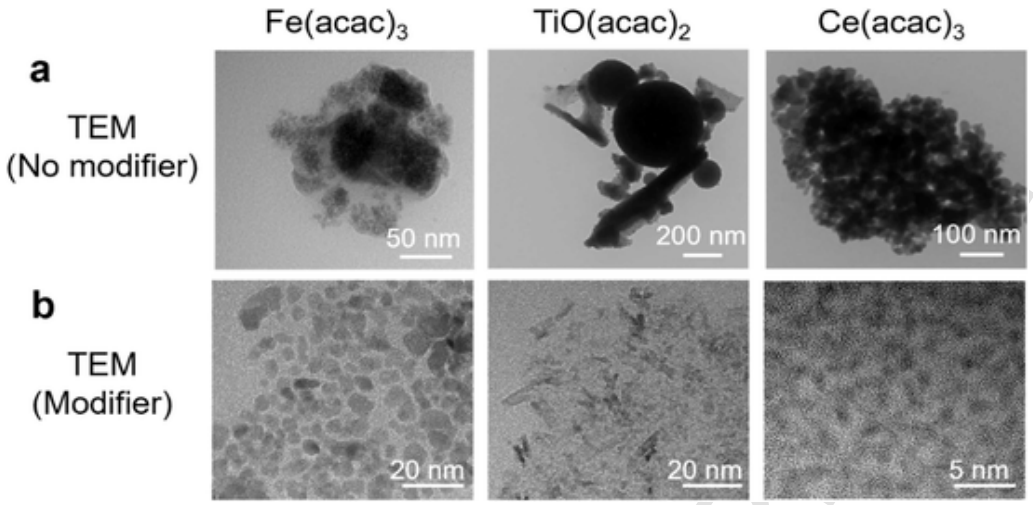

Fig. 1. TEM images of products synthesized (a) without surface modifier and (b) with surface modifier for $Fe(acac)_3$, $TiO(acac)_2$, and $Ce(acac)_3$ precursors.

making accurate determination of the mean size challenging. These results conclusively show that the addition of a surface modifier, oleic acid, was effective in inhibiting NP aggregation, allowing the synthesis of well-dispersed NPs.

Fig. 2 shows HR-TEM images and TEM-ED patterns of the product synthesized with the surface modifier. Fe, Ti, and Ce cases gave solid powders with colors similar to α-Fe_2O_3 (brown), TiO_2 (off-white), and CeO_2 (off-white), respectively. The HR-TEM images (Fig. 2**b**) showed multiple lattice fringes in all cases, indicating that the synthesized NPs had good crystallinity. The magnified HR-TEM images (Fig. 2**c**) of the Fe, Ti, and Ce cases revealed lattice spacings assignable to α-Fe_2O_3 of the hexagonal hematite structure (ICSD: 22505), TiO_2 of the tetragonal anatase structure (ICSD: 142916), and CeO_2 of the cubic fluorite structure (ICSD: 72155), respectively. In particular, HR-TEM analysis of the Ti sample revealed that the favored growth direction of anatase TiO_2 was along the c-axis of the tetragonal structure. The assigned crystal structures of the three products were also validated by the TEM-ED patterns (Fig. 2**d**), and each face spacing along with the assigned structure is listed in Table S1. The diffraction spots of Fe correspond to the face spacings of 0.383 nm, 0.289 nm, 0.263 nm, 0.233 nm, 0.179 nm,

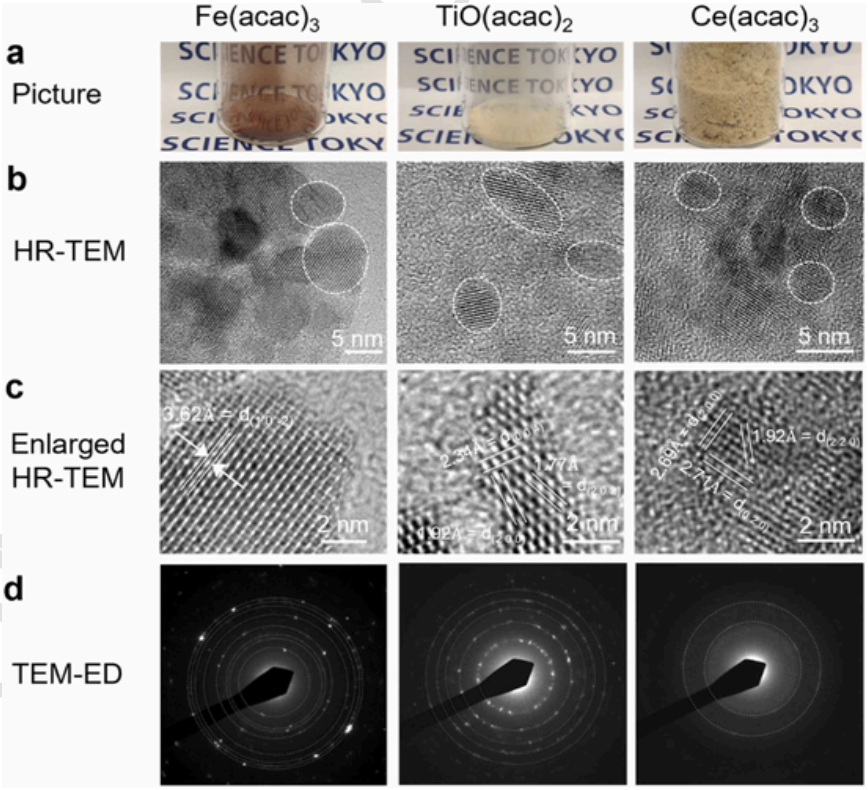

Fig. 2. Characterization results of products synthesized with surface modifiers for $Fe(acac)_3$, $TiO(acac)_2$, and $Ce(acac)_3$ precursors. (a) Photographs, (b) HR-TEM images, (c) magnified HR-TEM images, and (d) TEM-ED patterns.

0.161 nm, 0.154 nm, and 0.134 nm, which are assigned to α-Fe_2O_3. The diffraction spots of Ti correspond to face spacings of 0.359 nm, 0.243 nm, 0.194 nm, 0.171 nm, and 0.151 nm, which are assigned to TiO_2, while those of Ce correspond to face spacings of 0.280 nm and 0.196 nm, attributed to CeO_2. Therefore, $scCO_2$ media with oleic acid allows aggregation-free synthesis of α-Fe_2O_3, TiO_2, and CeO_2 NPs.

To analyze the surface structure, TG and FT-IR analyses applied to synthesized MONPs (α-Fe_2O_3, TiO_2, and CeO_2), as shown in Fig. 3. In the TG curve, the weight loss acceleration from 300 °C to 450 °C corresponded to the thermal decomposition of oleic acid [46]. This suggests that oleic acid is chemically attached to the surface of the NPs because the weight loss increase should cease near the boiling point of oleic acid (i.e., 285 °C) for physical adsorption [49,50]. The FT-IR spectra of the three products showed characteristic bands at 2900 cm^{-1} and 2850 cm^{-1}, which were assigned to the asymmetric and symmetric stretching modes of $–CH_2–$ in the alkyl chains of oleic acid [51]. The band of the free carboxyl group (–COOH) of oleic acid (usually detected at ~1700 cm^{-1}) was not confirmed in all products [51]. Instead, bands at approximately 1550 cm^{-1} and 1400 cm^{-1} emerged, which were assigned to the asymmetric and symmetric stretching vibrations of the carboxylate anion ($–COO^-$) in oleic acid, respectively [51]. These results evidentially show that oleic acid molecules are not physically adsorbed on the surface of these NPs, but rather chemically bonded to the surface [46]. Additionally, the separation of the asymmetric and symmetric stretching modes for $–COO^-$, Δ, was used to analyze the chemical bonding state of oleic acid in detail. The unidentate, bridging, and bidentate ligands are expected for Δ > 200 cm^{-1}, 200 cm^{-1} > Δ > 140 cm^{-1} and 110 cm^{-1} > Δ, respectively [52]. As shown in Fig. 3**c**, Fe shows two characteristic peaks at 1524 cm^{-1} and 1428 cm^{-1}, with a difference of 96 cm^{-1}, corresponding to the bidentate mode [53,54]. Ti gives rise to bands at 1526 cm^{-1}, 1436 cm^{-1}, and 1378 cm^{-1}, in which the difference between the band at 1526 cm^{-1} and other bands correspond to the bidentate (Δ = 90 cm^{-1}) and bridging (Δ = 148 cm^{-1}) modes, respectively. Ce also shows bands at 1525 cm^{-1}, 1459 cm^{-1}, and 1378 cm^{-1}, in which the difference between the band at 1525 cm^{-1} and other bands corresponds to the bidentate (Δ = 66 cm^{-1}) and bridging (Δ = 147 cm^{-1}) modes, respectively. These results indicate that oleic acid is chemically bonded to the surface of α-Fe_2O_3, TiO_2, and CeO_2 NPs as a bidentate, bidentate/bridging, and bidentate/bridging ligand, respectively, as shown in Fig. 3**d**. Thus, it can be concluded that oleic acid in $scCO_2$ successfully modifies the surface of α-Fe_2O_3, TiO_2, and CeO_2 NPs, allowing the synthesis of well-dispersed nanocrystals below 10 nm.

3.2. *Phase state observation for $Fe(acac)_3$, $TiO(acac)_2$, and $Ce(acac)_3$*

The phase state is important for the synthesis of surface-modified NPs because phase separation causes not only a low yield of the target product owing to the diffusion limit of the reactants but also induces the formation of undesirable byproducts in the separated phase [40,43]. In this work, the phase state during synthesis was analyzed for $Fe(acac)_3$, $TiO(acac)_2$ and $Ce(acac)_3$, as shown in Figs. 4**a** and 4**b**. The reactor contained solid $M(acac)_x$, liquid components (oleic acid, water, and ethanol), and a magnetic stirrer. Herein, whether the solid precursor is soluble in $scCO_2$ is important, as our previous research revealed the complete dissolution of liquid components in the same amounts under the same reaction conditions (30.0 MPa and 100 °C) [43]. In all three cases, the solid precursors completely dissolved into the $scCO_2$ phase at 30.0 MPa and 100 °C. Specifically, $Fe(acac)_3$ in the red powder, $TiO(acac)_2$ in the off-white powder, and $Ce(acac)_3$ in the yellow powder led to the formation of almost uniform reaction phases appearing orange, colorless, and light yellow in color. These phase behaviors indicate that $scCO_2$ combined with ethanol as an entrainer can sufficiently dissolve all three $M(acac)_x$ precursors, providing the homoge-

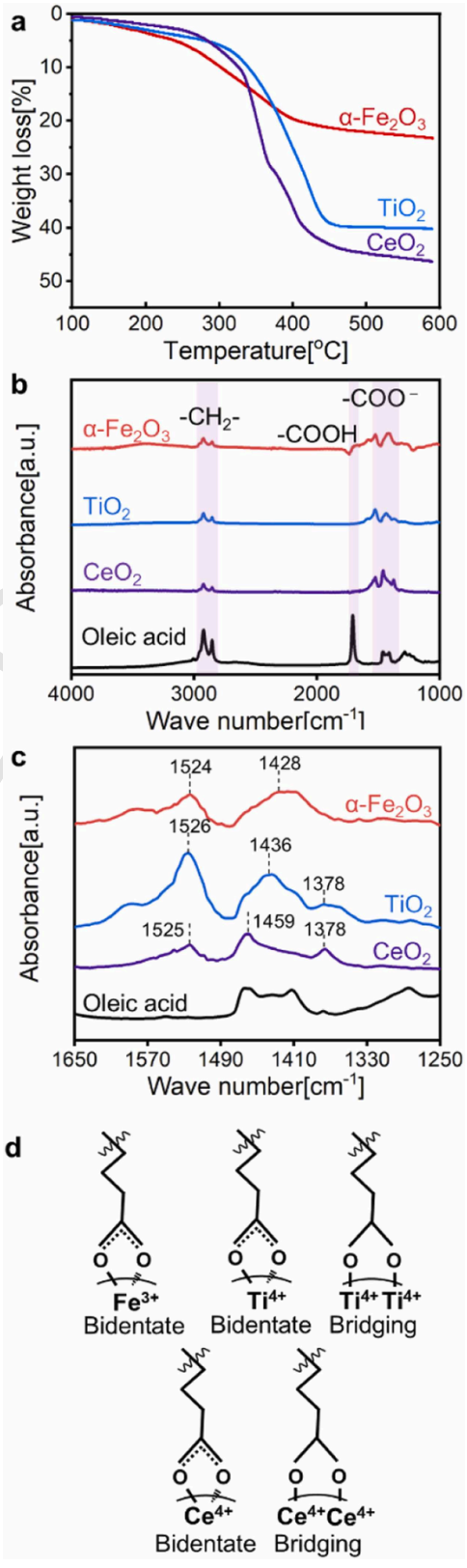

Fig. 3. Characterization results and estimated surface illustration of α-Fe_2O_3, TiO_2, and CeO_2 NPs synthesized with surface modifier. (a) TG curves, (b) FT-IR spectra, (c) magnified FT-IR spectra, and (d) estimated surface states.

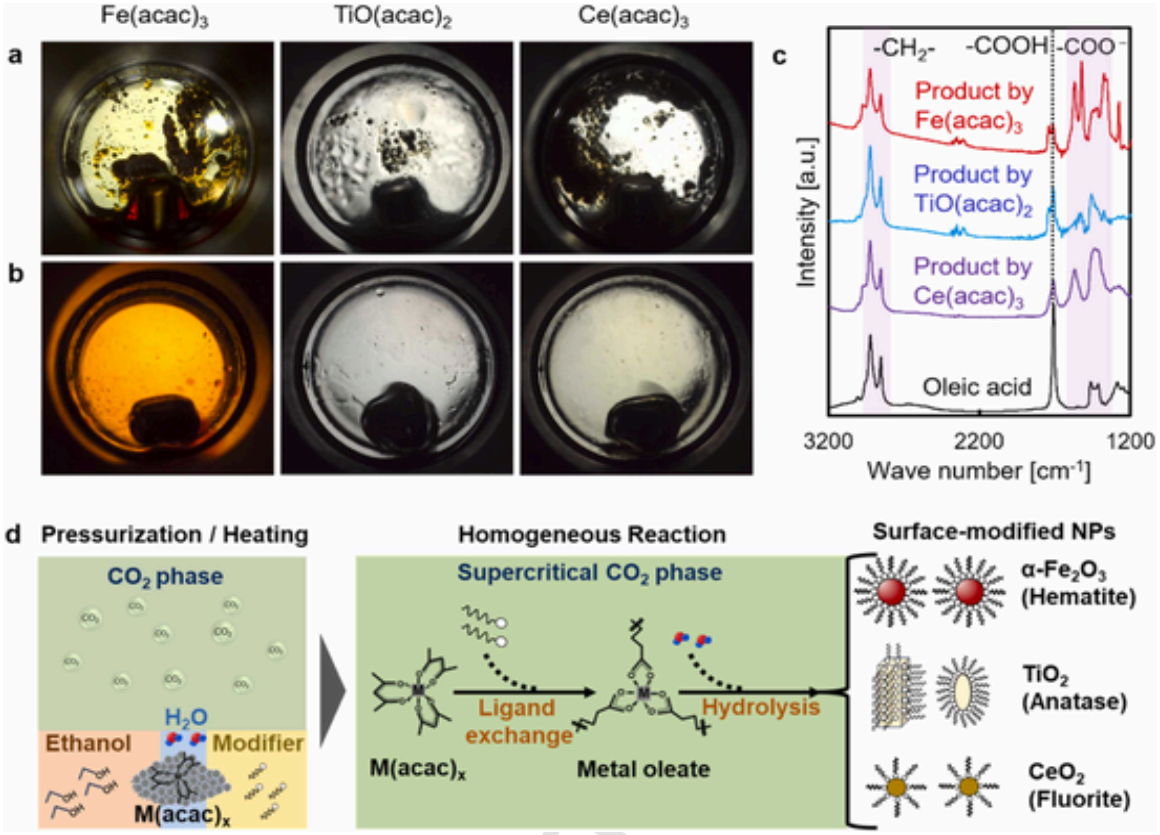

Fig. 4. Phase state (a) before pressurization/heating and (b) after pressurization/heating. (c) FT-IR spectra of products obtained without water addition and before post-treatment. (d) Proposed formation mechanism of various surface-modified NPs in $scCO_2$ atmosphere.

neous $scCO_2$ reaction field necessary for the successful synthesis of surface-modified NPs.

3.3. Proposed formation mechanism of surface-modified α-Fe_2O_3, TiO_2, and CeO_2 NPs

To clarify the role of water and validate the formation of metal oleate complexes for the synthesis of surface-modified α-Fe_2O_3, TiO_2, and CeO_2 NPs, syntheses were performed in $scCO_2$ (30.0 MPa and 100 °C) without water addition. Fig. 4**c** shows the FT-IR spectra of the product before post-treatment (washing and drying). All products showed the characteristic bands of –CH_2– (2900 cm^{-1} and 2850 cm^{-1}) and COO^- (1550 cm^{-1} and 1400 cm^{-1}) in oleic acid [51]. In addition, no solids (including metal oxide particles) were collected after washing with a hexane/acetone mixture. This result indicates that metal oxides were not formed in $scCO_2$ without water addition, which means that the thermolysis of metal precursors barely proceeds under our reaction conditions (100 °C, 18.0 h). Therefore, the –COO^- bands detected in the water-free system plausibly correspond to metal oleate complexes (formed via ligand exchange between $M(acac)_x$ and oleic acid), indicating that water is essential for the formation of metal oxide through the hydrolysis of metal oleate complexes.

Based on the above results, the formation mechanism of surface-modified NPs is proposed as follows (Fig. 4**d**): (1) Dissolution: Under elevated temperature and pressure, the reactants are gradually dissolved in $scCO_2$ to form a homogeneous reaction phase. Ethanol acts as an entrainer to enhance the solubility of the reactants, which is important because phase separation readily causes a low yield of the target product owing to the diffusion limit of the reactants and induces the formation of undesirable byproducts [40,43]. (2) Ligand exchange: Metal oleate complexes are formed via ligand exchange between $M(acac)_x$ and oleic acid. This step is critical because direct hydrolysis of $M(acac)_x$ would yield MONPs with hydrophilic surfaces, which are incompatible with the nonpolar $scCO_2$, resulting in severe aggregation [44]. (3) Formation: Hydrolysis of metal oleate complexes leads to the nucleation of surface-modified MONPs; oleic acid is chemically bonded to the MONP surfaces (as confirmed in Section 3.1). These NPs induce strong steric hindrance and have a hydrophobic surface compatible with $scCO_2$, which inhibits their aggregation.

3.4. Supercritical CO_2 treatment for $Co(acac)_3$, $Cr(acac)_3$, and $Ni(acac)_2$

To extract the key factor for the synthesis of surface modified NPs, same $scCO_2$ treatment with oleic acid was applied to $Co(acac)_3$, $Cr(acac)_3$, and $Ni(acac)_2$. Unlike $Fe(acac)_3$, $TiO(acac)_2$, and $Ce(acac)_3$, metal oxide crystals were not formed from these precursors. Fig. S2 summarizes the characterization results of the Co, Cr, and Ni products. TEM images (Fig. S2b) show the major products as irregularly shaped structures with vague boundaries in all cases. In addition, TEM-ED (Fig. S2c), and TEM-EDS (Fig. S2d) revealed that the products were amorphous structures composed of the corresponding metals (Co, Cr, or Ni), oxygen, and carbon. Furthermore, the TG curves (Fig. S2e) show weight losses of 72—81% between 100 °C and 600 °C, which is too high if metal oxides are the main products. Therefore, the major products are amorphous metal–organic complexes rather than metal oxide crystals. To investigate these complexes in detail, they were characterized by FT-IR spectroscopy (Fig. S2f). The FT-IR spectra showed characteristic bands (2900 cm^{-1} and 2850 cm^{-1}) derived from –CH_2– of oleic acid and characteristic bands (1550 cm^{-1} and 1400 cm^{-1}) derived from the carboxylate anion (–COO^-) in oleic acid [51]. In the absence of metal

oxide, these –COO^- bands are suggested to originate from metal oleate complexes. Thus, the detection of –COO^- indicates that the metal oleate is formed via ligand exchange between $M(acac)_x$ and oleic acid; however, the metal oleate does not hydrolyze to form metal oxides. The fact that no metal oxide NPs were formed for Co, Cr, and Ni is primarily attributed to the low hydrolytic activity of their respective metal oleate complexes in the $scCO_2$ system, which is in sharp contrast to the high hydrolytic activity of the Fe, Ti, and Ce precursors and complexes (Section 3.1).

3.5. Key factors for the synthesis of surface-modified NPs in $scCO_2$

The different reaction outcomes for the various metal precursors can be explained by the following mechanism: Fe, Ti, and Ce precursors can form metal oleate complexes with high hydrolytic activity, thus successfully yielding surface-modified MONPs. By contrast, Co, Cr, and Ni precursors form metal oleate complexes with low hydrolytic activity, leading to the absence of metal oxides (Section 3.4). Collectively, the formation and hydrolytic activity of metal oleate complexes are the key factors determining the success of surface-modified MONP synthesis in the $scCO_2$ system. If these conditions are satisfied, this method, which utilizes the hydrolysis of metal oleates in a homogenous $scCO_2$ field, is promising option for the green and efficient synthesis of well-dispersed MONPs.

4. Conclusion

In this study, we explored the universality of $scCO_2$ for the synthesis of various surface-modified MONPs. The syntheses were performed at 30.0 ± 0.5 MPa of CO_2 and 100 °C for 18.0 h using metal acetylacetonates (i.e., $Fe(acac)_3$, $TiO(acac)_2$, $Ce(acac)_3$, $Co(acac)_3$, $Cr(acac)_3$, and $Ni(acac)_2$), water, oleic acid, and ethanol as reactants. As a result, metal oxide crystals were not formed for Co, Cr, and Ni, while α-Fe_2O_3, TiO_2, and CeO_2 nanocrystals were successfully synthesized for Fe, Ti, and Ce. The addition of oleic acid to $scCO_2$ drastically inhibited the aggregation of α-Fe_2O_3, TiO_2, and CeO_2 nanocrystals by densely modifying their surfaces. Furthermore, according to the phase observations and metal oleate analysis, the formation of metal oleate and its hydrolytic activity are suggested to be key conditions for the successful synthesis of densely modified MONPs. These findings provide useful guidelines for exploring the universality of the $scCO_2$ process for various surface-modified MONPs and contribute to the development of green chemistry approaches using water and CO_2.

CRediT authorship contribution statement

Aoi Muronosono: Writing – review & editing, Validation, Methodology, Investigation. **Wenjing Hu:** Writing – original draft, Visualization, Validation, Methodology, Investigation. **Yi Liu:** Writing – review & editing, Supervision, Project administration. **Yamaguchi Yuki:** Writing – review & editing, Methodology, Investigation. **Yasuhiko Orita:** Writing – review & editing, Visualization, Validation, Supervision, Resources, Project administration, Methodology, Investigation, Funding acquisition, Conceptualization. **Yusuke Shimoyama:** Writing – review & editing, Validation, Supervision, Resources, Project administration.

Declaration of Competing Interest

The authors declare that they have no known competing financial interests or personal relationships that could have appeared to influence the work reported in this paper.

Acknowledgements

This study is based on results obtained from a project, JPNP23200871–0, subsidized by the New Energy and Industrial Technology Development Organization (NEDO). This work was supported by China Scholarship Council (CSC). TEM-related images were obtained from the Materials Analysis Division, Core Facility Center. We would like to thank Editage for English language editing.

Data Availability

The data that has been used is confidential.

Appendix A. Supporting information

Supplementary data associated with this article can be found in the online version at doi:10.1016/j.supflu.2026.107065.

References

[1] T. Tomai, N. Tajima, M. Kimura, A. Yoko, G. Seong, T. Adschiri, Solvent accommodation effect on dispersibility of metal oxide nanoparticle with chemisorbed organic shell, J. Colloid Interface Sci. 587 (2021) 574–580, https://doi.org/10.1016/j.jcis.2020.11.014.
[2] H. Li, Y. Zhu, Liquid-Phase Synthesis of Iron Oxide Nanostructured materials and their applications, Chem. Eur. J. 26 (2020) 9180–9205, https://doi.org/10.1002/chem.202000679.
[3] T. Teranishi, A. Sugawara, T. Shimizu, M. Miyake, Planar array of 1D gold nanoparticles on ridge-and-valley Structured Carbon, J. Am. Chem. Soc. 124 (2002) 4210–4211, https://doi.org/10.1021/ja017536k.
[4] S. Tanaka, Y.V. Kaneti, N.L.W. Septiani, S.X. Dou, Y. Bando, M.S.A. Hossain, J. Kim, Y. Yamauchi, A review on iron oxide-based nanoarchitectures for biomedical, energy storage, and environmental applications, small Methods 3 (2019) 1800512, https://doi.org/10.1002/smtd.201800512.
[5] R. Mout, D.F. Moyano, S. Ranaa, V.M. Rotello, Surface functionalization of nanoparticles for nanomedicine, Chem. Soc. Rev. 41 (2012) 2539–2544, https://doi.org/10.1039/C2CS15294K.
[6] I. Lynch, K.A. Dawson, Protein-nanoparticle interactions, Nano Today 3 (2008) 40–47, https://doi.org/10.1016/S1748-0132(08)70014-8.
[7] J. Shi, P.W. Kantoff, R. Wooster, O.C. Farokhzad, Cancer nanomedicine: progress, challenges and opportunities, Nat. Rev. Cancer 17 (2017) 20–37, https://doi.org/10.1038/nrc.2016.108.
[8] M.W. Alam, R. Ambikapathi, S. Nabi, A. Nivetha, B. Abebe, H.H. Almutairi, S. Sadaf, S.M. Almohish, Advancements in green-synthesized transition metal/metal-oxide nanoparticles for sustainable wastewater treatment: techniques, applications, and future prospects, Mater. Res. Express 11 (2024) 102001, https://doi.org/10.1088/2053-1591/ad86a4.
[9] S. Payamifara, M. Abdoussa, A.P. Marjani, The application of magnetic nanoparticles based β-cyclodextrin as recoverable catalyst in various organic transformations: An overview, Arab. J. Chem. 18 (2025) 106080, https://doi.org/10.1016/j.arabjc.2024.106080.
[10] W. Li, Y. Liu, Y. Zhao, W. Yan, J. Hu, J. Ma, K. Zhang, W. Yang, Decoration of CeO_2 nanoparticles on Cu/Co bimetallic oxide and their catalytic performance, Mater. Today Chem. 42 (2024) 102368, https://doi.org/10.1016/j.mtchem.2024.102368.
[11] L. Nikola, R. Piech, C. Wardak, B. Paczosa-Bator, Application of metal oxide nanoparticles in the field of potentiometric sensors: A Review, Membranes 13 (2023) 876, https://doi.org/10.3390/membranes13110876.
[12] P.D. Howes, R. Chandrawati, M.M. Stevens, Colloidal nanoparticles as advanced biological sensors, Science 346 (2014) 1247390, https://doi.org/10.1126/science.1247390.
[13] C. Ungureanu, G.T. Tihan, R.G. Zgârian, I. Fierascu, A.M. Baroi, S. Răileanu, R.C. Fierăscu, Metallic and metal oxides nanoparticles for sensing food pathogens-an overview of recent findings and future prospects, Materials 15 (2022) 5374, https://doi.org/10.3390/ma15155374.
[14] C. Wroblewski, R.I. Barbhuiya, G. Kaur, G.R. Nair, A. Elsayed, A. Singh, A comprehensive insight into metal oxide nanoparticle synthesis, associated regulations, and application in the agri-food sector, Can. J. Chem. Eng. 103 (2025) 1736–1751, https://doi.org/10.1002/cjce.25484.
[15] M.M. Ahmad, M. Shehla, H.S.A. Qahtan, A. Sedky, M.W. Alam, Investigation of TiO_2 nanoparticles synthesized by sol-gel method for effectual photodegradation, oxidation and reduction reaction, Crystals 11 (2021) 1456, https://doi.org/10.3390/cryst11121456.
[16] K. Xia, G.T. Fei, S.H. Xu, X.D. Gao, Y.F. Liang, Hot-injection synthesis of HgTe nanoparticles: Shape control and growth mechanisms, Inorg. Chem. 62 (2023) 13632–13638, https://doi.org/10.1021/acs.inorgchem.3c02030.
[17] H. Singh, S. Kour, M. Selvaraj, Magnetically separable template assisted iron nanoparticle for the enhancement of latent fingerprints, J. Indian. Chem. Soc. 99 (2022) 100661, https://doi.org/10.1016/j.jics.2022.100661.
[18] J. Muro-Cruces, A.G. Roca, A. Lo´pez-Ortega, E. Fantechi, D. Del-Pozo-Bueno, S.

Estrad´e, F. Peiro´, B. Sepúlveda, F. Pineider, C. Sangregorio, J. Nogues, Precise size control of the growth of Fe_3O_4 nanocubes over a wide size range using a rationally designed one-pot synthesis, ACS Nano 13 (2019) 7716–7728, https://doi.org/10.1021/acsnano.9b01281.
[19] H. Kasai, K. Maeda, E. Nishibori, Reaction pathway in the hydrothermal synthesis of metal nanoparticles using formic acid, ACS Appl. NanoMater. 7 (2024) 26698–26705, https://doi.org/10.1021/acsanm.4c03972.
[20] Y. Ioni, A. Popova, S. Maksimov, I. Kozerozhets, Ni nanoparticles on the reduced graphene oxide surface synthesized in supercritical isopropanol, Nanomaterials 13 (2023) 2923, https://doi.org/10.3390/nano13222923.
[21] M. Ahmed, S.A. Mahmoud, A.A. Mohamed, Interfacially engineered metal oxide nanocomposites for enhanced photocatalytic degradation of pollutants and energy applications, RSC Adv. 15 (2025) 15561–15603, https://doi.org/10.1039/D4RA08780A.
[22] A. Refia, R. Islam, M.A. Gonzalez, P. Chinwangso, T.R. Lee, Recent advances in polymer-coated metal and metal oxide nanoparticles: From design to promising applications, Nanomaterials 15 (2025) 1744, https://doi.org/10.3390/nano15221744.
[23] Z.S. Tahseen, B.Z. Rashid, S.H. Ali, K.N. Kaka, S.J. Salih, Next-generation Ni-doped $CoFe_2O_4$@SiO_2-NH_2-gallic acid nanocomposites: Synergistic effects of functionalization for advanced dye removal and antibacterial applications, J. Hazard. Mater. Adv. 18 (2025) 100686, https://doi.org/10.1016/j.hazadv.2025.100686.
[24] B. Geng, X. Liu, J. Ma, Q. Du, A new nonhydrolytic single-precursor approach to surfactant-capped nanocrystals of transition metal sulfides, Mater. Sci. Eng. B 145 (2007) 17–22, https://doi.org/10.1016/j.mseb.2007.09.065.
[25] J. Zhang, S. Ohara, M. Umetsu, T. Naka, Y. Hatakeyama, T. Adschiri, Colloidal ceria nanocrystals: a tailor-made crystal morphology in supercritical water, Adv. Mater. 19 (2007) 203–206, https://doi.org/10.1002/adma.200600964.
[26] E. Scopel, P.P. Conti, D.G. Stroppa, C.J. Dalmaschio, Synthesis of functionalized magnetite nanoparticles using only oleic acid and iron (III) acetylacetonate, SN Appl. Sci. 1 (2019) 147, https://doi.org/10.1007/s42452-018-0140-6.
[27] Y.V. Kolen'Ko, M. Ban˜obre-Lo´pez, C. Rodríguez-Abreu, E. Carbo´-Argibay, A. Sailsman, Y. Pineiro-Redondo, M.F. Cerqueira, D.Y. Petrovykh, K. Kovnir, O.I. Lebedev, J. Rivas, Large scale synthesis of colloidal Fe_3O_4 nanoparticles exhibiting high heating efficiency in magnetic hyperthermia, J. Phys. Chem. C. 118 (2014) 8691–8701, https://doi.org/10.1021/jp500816u.
[28] K. Nakaso, B. Han, K.H. Ahn, M. Choi, K. Okuyama, Synthesis of non-agglomerated nanoparticles by an electrospray assisted chemical vapor deposition (ES-CVD) method, J. Aerosol Sci. 34 (2003) 869–881, https://doi.org/10.1016/S0021-8502(03)00053-3.
[29] X.C. Yang, W. Riehemann, M. Dubiel, H. Hofmeister, Nanoscaled ceramic powders produced by laser ablation, Mater. Sci. Eng. B 95 (2002) 299–307, https://doi.org/10.1016/S0921-5107(02)00291-X.
[30] S.J. Hong, J.I. Han, Synthesis and characterization of indium tin oxide (ITO) nanoparticle using gas evaporation process, J. Electroceram. 17 (2006) 821–826, https://doi.org/10.1007/s10832-006-9332-3.
[31] J.G. Mattei, P. Grammatikopoulos, J. Zhao, V. Singh, J. Vernieres, S. Steinhauer, A. Porkovich, E. Danielson, K. Nordlund, F. Djurabekova, M. Sowwan, Gas-phase synthesis of trimetallic nanoparticles, Chem. Mater. 31 (2019) 2151–2163, https://doi.org/10.1021/acs.chemmater.9b00129.
[32] A. Gutsch, M. Kramer, G. Michael, H. Muhlenweg, M. Pridohl, G. Zimmermann, Gas-phase production of nanoparticles, KONA Powder Part. J. 20 (2002) 24–37, https://doi.org/10.14356/kona.2002008.
[33] Y. Yang, W. Li, Gas phase nanoparticle formation, in: B. Bhushan (Ed.), Encyclopedia of nanotechnology, 2012, pp. 929–933, https://doi.org/10.1007/978-90-481-9751-4_358.
[34] M. Kinoshita, Y. Shimoyama, Dynamic phase behavior during sol-gel reaction in supercritical carbon dioxide for morphological design of nanostructured titania, J. Supercrit. Fluids 116 (2016) 190–197, https://doi.org/10.1016/j.supffu.2016.05.008.
[35] Y. Murakami, K. Inoue, R. Akiyama, Y. Orita, Y. Shimoyama, LipTube: Liposome formation in tube process using supercritical CO_2, Ind. Eng. Chem. Res. 61 (2022) 14598–14608, https://doi.org/10.1021/acs.iecr.2c02095.
[36] R. Akiyama, Y. Murakami, K. Inoue, Y. Orita, Y. Shimoyama, Fabrication of PEGylated liposome in microfluidic flow process using supercritical CO_2, J. Nanopart. Res. 24 (2022) 257, https://doi.org/10.1007/s11051-022-05635-9.
[37] K. Ikeda, Y. Shimoyama, Y. Orita, Efficient purification of surface modified nanoparticles from its nanosuspension by using supercritical CO_2 technology, J. Supercrit. Fluids 199 (2023), 105966 https://doi.org/10.1016/j, supffu.2023.105966.
[38] M. Haruki, F. Kobayashi, S.I. Kihara, S. Takishima, Effect of the chemical structures of iron complexes on the solubilities in supercritical carbon dioxide, Fluid. Phase Equilib. 308 (2011) 1–7, https://doi.org/10.1016/j.ffuid.2011.05.008.
[39] X. Zhang, S. Heinonen, E. Levänen, Applications of supercritical carbon dioxide in materials processing and synthesis, RSC Adv. 4 (2014) 61137–61152, https://doi.org/10.1039/C4RA10662H.
[40] Y. Orita, K. Kariya, T. Wijakmatee, Y. Shimoyama, Synthesis of surface-modified iron oxide nanocrystals using supercritical carbon dioxide as the reaction field, RSC Adv. 12 (2022) 7990–7995, https://doi.org/10.1039/d1ra08580h.
[41] M.K.M. Lane, J.B. Zimmerman, Controlling metal oxide nanoparticle size and shape with supercritical fluid synthesis, Green. Chem. 21 (2019) 3769–3781, https://doi.org/10.1039/C9GC01619H.
[42] T. Furuya, Y. Shimoyama, Y. Orita, Low temperature synthesis of ZnO particles using a CO_2-driven mechanism under high pressure, RSC Adv. 14 (2024) 5176–5183, https://doi.org/10.1039/D3RA07067K.
[43] A. Muronosono, T. Furuya, Y. Shimoyama, Y. Orita, High-concentrated synthesis of surface modified iron oxide nanoparticles using ethanol-enhanced supercritical CO_2 media, Colloid Surf. A Physicochem. Eng. Asp. 705 (2025) 135650, https://doi.org/10.1016/j.colsurfa.2024.135650.
[44] Y. Orita, K. Kariya, T. Wijakmatee, Y. Shimoyama, Formation mechanism of iron oxide nanoparticles using controlled hydrolysis reaction in supercritical carbon dioxide, Colloid Surf. A Physicochem. Eng. Asp. 664 (2023) 131136, https://doi.org/10.1016/j.colsurfa.2023.131136.
[45] T. Wijakmatee, Y. Shimoyama, Y. Orita, Systematically designed surface and morphology of magnetite nanoparticles using monocarboxylic acid with various chain lengths under hydrothermal condition, Langmuir 39 (2023) 9253–9261, https://doi.org/10.1021/acs.langmuir.3c01225.
[46] M. Taguchi, N. Yamamoto, D. Hojo, S. Takami, T. Adschiri, T. Funazukuria, T. Naka, Synthesis of monocarboxylic acid-modified CeO_2 nanoparticles using supercritical water, RSC Adv. 4 (2014) 49605–49613, https://doi.org/10.1039/C4RA06936F.
[47] A.S. Khodkina, M.A. Ovchinnikov, I.E. Rasskazov, A.V. Kolchin, D.V. Korolev, E.I. Kunitsyna, M.V. Bakhmetiev, S.I. Serebrennikova, V. Ibragimova, N.D. Mitiushev, E.N. Kabachkov, F.S. Fedorov, A.G. Nasibulin, Y.V. Ioni, Synthesis of hybrid materials based on reduced graphene oxide and Ni (NiO) nanoparticles by supercritical solvent and thermal treatment techniques, Mater. Sci. Eng. B 324 (2026) 118950, https://doi.org/10.1016/j.mseb.2025.118950.
[48] Y. Koga, Y. Iwai, Y. Hata, M. Yamamoto, Y. Arai, Influence of cosolvent on solubilities of fatty acids and higher alcohols in supercritical carbon dioxide, Fluid. Phase Equilib. 125 (1–2) (1996) 115–128, https://doi.org/10.1016/S0378-3812(96)03090-7.
[49] M. Taguchi, S. Takami, T. Naka, T. Adschiri, Growth mechanism and surface characteristics of dicarboxylic acid-modified CeO_2 nanocrystals produced in supercritical water: Tailor-made water-soluble CeO_2 nanocrystals, Cryst. Growth Des. 9 (2009) 5297–5303, https://doi.org/10.1021/cg900809b.
[50] M. Taguchi, S. Takami, T. Adschiri, T. Nakane, K. Sato, T. Naka, Supercritical hydrothermal synthesis of hydrophilic polymer-modified water-dispersible CeO_2 nanoparticles, CrystEngComm 13 (2011) 2841–2848, https://doi.org/10.1039/C0CE00467G.
[51] K. Nakanishi, Infrared absorption spectroscopy: practical, Holden-Day, San Francisco, 648-648. Science. 140 (1963), https://doi.org/10.1126/science.140.3567.648.a.
[52] K. Nakamoto, Infrared and raman spectra of inorganic and coordination compounds, J. Chem. Educ. 56 (5) (1979), https://doi.org/10.1021/ed056pA209.
[53] S.J. Kemp, R.M. Ferguson, A.P. Khandhar, K.M. Krishnan, Monodisperse magnetite nanoparticles with nearly ideal saturation magnetization, RSC Adv. 6 (2016) 77452–77464, https://doi.org/10.1039/c6ra12072e.
[54] L.M. Bronstein, X. Huang, J. Retrum, A. Schmucker, M. Pink, B.D. Stein, B. Dragnea, Influence of iron oleate complex structure on iron oxide nanoparticle formation, Chem. Mater. 19 (2007) 3624–3632, https://doi.org/10.1021/cm062948j.